

**Droplet CAR-Wash: Continuous Picoliter-Scale Immunocapture and Washing**

Journal:	<i>Lab on a Chip</i>
Manuscript ID	LC-ART-02-2019-000125.R1
Article Type:	Paper
Date Submitted by the Author:	18-Mar-2019
Complete List of Authors:	Doonan, Steven; University of Michigan, Department of Chemistry Lin, Melissa; University of Michigan, Department of Chemistry Bailey, Ryan; University of Michigan, Department of Chemistry

Droplet CAR-Wash: Continuous Picoliter-Scale Immunocapture and Washing

Steven R. Doonan,¹ Melissa Lin,¹ and Ryan C. Bailey^{1,*}

¹Department of Chemistry, University of Michigan, Ann Arbor, MI 48109

*ryancb@umich.edu

†Electronic Supplementary Information (ESI) is available.

Abstract:

To address current limitations in adapting solid phase sample capture and washing techniques to continuously flowing droplet microfluidics, we have developed the “Coalesce-Attract-Resegment Wash” (CAR-Wash) approach. This module provides efficient, high-throughput magnetic washing by electrocoalescing magnetic bead-laden input droplets with a washing buffer flow and magnetophoretically transporting beads through the buffer into a secondary droplet formation streamline. In this work, we first characterized the technology in terms of throughput, sample retention, and flow-based exclusion of waste volume, demonstrating >500 Hz droplet processing with >98% bead retention and >100-fold dilution in final droplets. Next, we showed that the technique can be adapted to alternative commercially available magnetic beads with lower magnetite content per particle. Then, we demonstrated the CAR-Wash module’s effectiveness in washing away a small molecule competitive inhibitor to restore the activity of magnetic bead-immobilized β -galactosidase. Finally, we applied the system to immunomagnetically enrich a Green Fluorescent Protein-Histone H2B fusion protein from cell lysate while washing away mCherry and other lysate components. We believe this approach will bridge the gap between powerful biochemical and bioanalytical techniques and current droplet microfluidic capabilities, and we envision future application in droplet-based immunoassays, solid phase extraction, and other complex, multi-step operations.

Introduction:

Droplet microfluidics have enabled revolutionary miniaturization capabilities for chemistry and biochemistry. By compartmentalizing samples in oil, two-phase segmented flow systems enable the automated handling of discretized samples through complex operations at rates of up to several kHz.¹⁻⁴ Individual droplets (fL-nL in volume) experience rapid mass transfer due to internal convective flows and short mixing distances, enhancing the speed and efficiency of in-droplet chemistry.^{2, 3, 5} By leveraging fluorinated oils and optimized surfactants, these systems allow stable droplet production, extended storage, and sophisticated manipulation to provide performance analogous to or exceeding that of many bulk assays.⁶ Further, the power of handling large numbers of discrete, often heterogeneous sample volumes through miniaturized, rapid processing has uniquely poised droplet microfluidics at the forefront of several exciting biochemical developments. As recent examples, droplet technologies have achieved single-nucleus RNA sequencing,⁷ epigenetic analysis of nucleosome positioning,⁸ and directed enzyme evolution,⁹ among other implementations. A number of reviews profile notable droplet applications in detail.^{2, 4, 10-12}

Beyond these developments, integrating solid phase sample capture and manipulation can significantly extend the capabilities of microfluidics.^{4, 13-16} This class of sample processing is ubiquitous in chemistry and biochemistry, retaining selected targets on a solid phase by immobilizing antibodies or complementary oligonucleotide sequences, by manipulating surface chemistry, or by using other approaches while allowing for the exchange or washing of buffers, reagents, and off-target species.¹⁷⁻²¹ Clearly, sample immobilization and washing via interactions with a solid phase provides a range of important opportunities in synthesis, pre-concentration, extraction, and analytical measurements.^{4, 13, 15} For example, a powerful bioanalytical technique, the (heterogeneous phase) immunoassay, leverages a sequence of washing and reagent exchange steps to provide an important method for clinical protein quantitation.^{13, 18} To empower these capabilities in integrated droplet-based microfluidic devices, magnetic fields have provided a popular choice of flow-orthogonal force for selective manipulation of the solid phase.^{4, 13, 16} Successful techniques include magnetic droplet translation through a series of co-flowing laminar reagent streams for applying polyelectrolyte surface coatings,^{22, 23} magnetic tweezers for

immobilizing bead volumes while exchanging reagent droplets around them for multistep bioassays,^{24, 25} and additional examples of ferrofluid dispersed or continuous phase components for droplet generation and manipulation.^{26, 27} These approaches have demonstrated efficient and selective magnetic phase manipulation for a range of applications, but additional capabilities are needed to fully adapt solid phase (bio)chemical techniques into droplet microfluidics.

Unfortunately for continuously flowing droplet technologies a key deficiency remains. Although well-characterized strategies in a range of material systems²⁸ continuously and reliably form droplets and add reagents using T-junctions,²⁹ pairwise droplet fusion,¹⁴ picoinjectors,³⁰ and other modules,^{2, 3, 31, 32} approaches for selective sample capture and washing have faced serious limitations. The most prevalent scheme for in-droplet sample purification combines droplet splitting with a channel-adjacent magnetic field, concentrating magnetic bead-tethered sample in only one of the daughter droplets. A range of variations on this approach have achieved limited success within a few analytical applications. Examples have demonstrated high magnetic bead recovery, removal of up to 95% of starting waste volume through droplet splitting asymmetry, and/or low to modest throughput (0.5-200 Hz droplet frequencies).^{17, 31, 33-37} Nonetheless, this approach can require serial droplet splitting and reagent addition operations (with exponentially decreasing effect) to reach higher washing purity, increasing device complexity while decreasing throughput.^{35, 36} Lee *et al.* proposed an interesting alternative: collecting magnetic beads in a washing buffer droplet during temporary fusion with the original bead-laden sample droplet.¹⁴ This was followed by nearly immediate breakup into the two original component droplets. While this device achieved approximately 25-fold dilution and bead transfer into collected droplets with little sample loss, it was also hindered by reduced throughput (3 Hz reported) and the added complexity of droplet synchronization for pairwise fusion and breakup. Finally, Alorabi *et al.* showed an impressive example of magnetic washing using multilaminar flow for magnetic droplet processing.²² This device demonstrated effective washing by magnetically pulling entire ferrofluid droplets across orthogonally flowing washing buffer streams during a sophisticated layer by layer surface functionalization, in contrast to the discrete washing volumes involved in other droplet washing strategies. Recent reviews profile the breadth of solid phase manipulations in

droplets, including alternative washing technologies to the continuously flowing droplet systems described here.^{4, 13} These alternatives include micropillar and microwell-based devices,^{38, 39} acoustic and magnetic systems for temporary bead trapping (like those described above),^{24, 25, 40} and digital microfluidic (DMF) strategies.⁴¹ Such techniques, however, sacrifice the throughput and mixing characteristics common to continuously flowing droplet systems. A clear need for high speed, high efficiency in-droplet washing technologies remains.

In this work we sought to develop an efficient washing device without compromising simplicity of operation and droplet processing throughput. Our “Coalesce-Attract-Resegment Wash” (CAR-Wash) approach leverages a combination of electric and magnetic fields to fuse input droplets and then generate new droplets from a continuous washing buffer flow while capturing magnetic particles selectively in those final droplets. Thus, we realized greater than 100-fold dilution of the original droplets with minimal magnetic particle loss. Importantly, this technique operates at hundreds of Hz droplet frequencies, making it compatible with the high frequencies of many other droplet operations. Finally, we applied this technique to washing away a small molecule inhibitor to restore enzyme activity and to perform a selective protein enrichment and purification from cell lysate.

Experimental:

Microfluidic Device Preparation. Devices were fabricated using standard soft lithography.⁴² In brief, SU8 2025 Negative Epoxy Photoresist (MicroChem Corp.) was spin coated to 40 μm thickness on silicon wafers (University Wafer). Devices were designed in AutoCAD software (Autodesk, Inc.) and sourced as transparencies (CAD/Art Services, Inc.) for use in photolithography. After wafer baking and development, masters were surface treated under vacuum with tridecafluoro-1,1,2,2-tetrahydrooctyl trichlorosilane (Gelest, Inc.) prior to use. A 5:1 base:curing agent ratio was used to fabricate PDMS (RTV615, Momentive Performance Materials, Inc.) devices that were bonded to glass cover slips (Sigma Aldrich) via oxygen plasma activation (PDC-32G, Harrick Plasma, Inc.) after punching inlet ports with a 30 gauge needle. All channels were 40 μm in depth and 40-200 μm in width. Devices were treated with 1% tridecafluoro-1,1,2,2-tetrahydrooctyl trichlorosilane in Fluoroinert FC-40 (Sigma Aldrich) prior to use.

Flow Control. Flow control on-device used a custom pressure controller. Nitrogen gas was directed through a splitting manifold to an array of two-stage regulators (VWR International) which selected applied pressures. From the regulators, gas was directed into a network of LHDA0531115H solenoid valves (The Lee Company) actuated by LabView via a NI PCIe-6251 Multifunction Data Acquisition Device (National Instruments Corporation). Finally, this gas was delivered through stainless steel pins (New England Small Tube Corporation) into the headspace of solution-filled reservoir vials connected to microfluidic device inlets through lengths of #30 PTFE tubing (Cole-Parmer). Applied pressures were between 10 and 100 kPa, yielding typical flow rates on the scale of $\mu\text{L}/\text{min}$. For example, the 500 Hz operation shown in Figure 2 applied 55 kPa to the washing buffer, 45 kPa to the oil co-flow, 65 kPa to the input droplets, and 10 kPa to the waste outlet. This resulted in approximate flow rates of 75 $\mu\text{L}/\text{min}$ for washing buffer, 8.5 $\mu\text{L}/\text{min}$ for the oil co-flow, and 4.5 $\mu\text{L}/\text{min}$ for input droplets.

Electric and Magnetic Fields. Electric field was generated using a custom inverter to apply ~ 45 VAC (36 kHz) to the device. Electric field was connected via a submerged platinum wire in the washing buffer reservoir and via a syringe with 3M NaCl used to fill saline electrode channels (40 μm channel depth).⁴³ Magnetic field was provided by an array of eight grade N52 NdFeB 1/2" x 1/4" x 1/8" magnets (K&J Magnetics, Inc.) positioned 200-500 μm from the channel using microfabricated alignment marks, and magnetization was directed toward the separation channel.

Reagents and Sample Preparation. Magnetic beads were Streptavidin Microparticles, 10 μm particle size (Sigma Aldrich), or Protein G Dynabeads, 2.8 μm particle size (Thermo Fisher Scientific). Beads were rinsed in water or buffer and re-suspended prior to use. For device characterization experiments, magnetic beads were re-suspended in 1 mM fluorescein (Sigma Aldrich) in water with 60% Optiprep (Sigma Aldrich) and 20% PBS, and the washing buffer was PBS. The fluorescent standard for these experiments was 10 μM fluorescein in PBS, and the continuous phase oil was 1% or 2% 008-Fluorosurfactant (Ran Biotechnologies, Inc.) in Novec 7500 (The 3M Company).

For the enzyme inhibition assay, 10 μg β -Galactosidase-biotin labeled from *Escherichia coli* (Sigma Aldrich) was incubated on 10 μm streptavidin microparticles for 2 hours then washed to remove

unbound enzyme and re-suspended in 60% optiprep with 40% PBS and 0.2% BSA. Substrate (used as washing buffer) was 500 nM resorufin- β -D-galactopyranoside (Thermo Fisher Scientific) prepared in PBS, 0.5% BSA. Initial droplets or substrate with inhibitor also contained 1 mM isopropyl β -D-1-thiogalactopyranoside (IPTG) (Thermo Fisher Scientific) as indicated.

For the fluorescent protein enrichment assay, the cells were HeLa with Green Fluorescent Protein-Histone H2B (GFP-H2B) fusion expressed. Briefly, the cell sample processing procedure included bulk lysis and enzymatic chromatin digestion of \sim 250,000 cells in detergent-rich Lysis and Digestion Buffers with Micrococcal Nuclease (New England BioLabs) as described previously.⁸ mCherry (BioVision, Inc.) was added to 3.3 μ g/mL for the final cell lysate suspension. Anti-GFP beads were prepared using 10 μ m streptavidin microparticles with 4.5 μ g GFP Rabbit anti-Jellyfish, Polyclonal Antibody (Thermo Fisher Scientific) following biotinylation of the antibody according to manufacturer's protocols (EZ-Link Sulfo-NHS-LC-Biotin, Thermo Fisher Scientific). After overnight incubation in 10 mM HEPES, 150 mM NaCl, 50 mM EDTA, 0.1% PEG, pH 7.4, beads were manually washed and re-suspended in a fresh aliquot of the same buffer to remove unbound antibodies. This buffer was also used as the washing buffer during device operation.

Data Collection and Analysis. Images were collected using a VEO 640L high speed camera (Vision Research Inc.) connected to a DMI8 light microscope (Leica Microsystems). Fluorescent imaging was performed using a FITC filter cube for the green channel and a TXR filter cube for the red channel (Leica Microsystems). Image processing and analysis were performed using ImageJ software (NIH). Droplet size, spacing, and frequency and magnetic particle position were manually determined from brightfield images. Flow rates were calculated from droplet size, spacing, and frequency and particle velocity down the channel length. For evaluating magnetic migration velocity, particle trajectories were divided into five bins based on particle starting position in the y (magnet-oriented) direction. Magnetic migration velocity calculations compared the average velocity values for each bin after discarding the bin containing the washing buffer-oil co-flow interface (where magnetically-induced particle migration was restricted by the interface). Representative fluorescent images in figures were uniformly adjusted in

brightness by fluorescent channel for ease of visualization, but quantitative data were obtained from the original images. For device characterization, droplet fluorescence localization plots average $N = 20$ time-points each, and the final plots were smoothed using a five point moving average. Plots of intensity values for the enzyme inhibition and fluorescent protein enrichment assays provide representative results for at least $N = 50$ droplets or beads for each reported sub-population. Statistical significance was assessed using a two sample Student's t-Test with a 95% confidence significance threshold (significance indicated by a dashed red line or an asterisk in plots).

Results and discussion:

CAR-Wash Operating Principles. To provide a simple, robust, and effective droplet-based magnetic purification and washing method, we developed the “Coalesce-Attract-Resegment Wash” (CAR-Wash) platform. The main operating principles for this technique are highlighted in Figure 1. Droplets containing the magnetic bead solid phase enter the device and are subject to a destabilizing electric field. This field triggers droplet coalescence with a parallel washing buffer stream and can be generated on-device by directly charging a suitably conductive washing buffer and/or through conventional electrolyte-filled microchannel features.⁴³ As the boundaries between each input droplet and the washing buffer fuse, superparamagnetic beads escape the original droplet volume under the attractive influence of a channel-adjacent permanent magnet. While the laminar flow condition confines the input droplet fluid to its original streamline with relatively little mixing into the buffer flow, magnetic beads fully translate across the channel width. An oil co-flow provides a moving boundary to stop beads from reaching the channel wall while keeping them moving toward the end of the module. In the absence of this co-flow, beads may be trapped under the combined influence of maximum magnetic field and minimum orthogonal flow forces in the near-zero slip flow at the channel wall. Finally, the majority of channel flow diverts to waste (containing the input droplet volume and much of the washing buffer), and the streamline with magnetic beads segments into new droplets in combination with the oil co-flow. The abrupt local decrease in channel cross section and dispersed phase flow rate drives stable droplet formation in a dripping regime (under typical flow conditions).³² Resegmented bead-containing droplets (now comprised of washing buffer) are suitable for

further downstream processing, including, but not limited to, additional CAR-Wash operations for sequential buffer exchange.

Beyond this qualitative description of CAR-Wash operation, we also examined the physical principles interacting with parameters such as magnetic field, flow conditions, and magnetic bead identity. Each contributes to magnetic particle trajectory through the device, so we probed the effects of these parameters on the relative magnitudes of each force and the relative magnitudes of each force per unit particle mass (in examining different bead sizes). First, the magnetic component of particle motion under a constant, high magnetic field is described under conditions of uniformly saturated magnetization throughout the particle:

$$\mathbf{F}_m = \left(\frac{1}{\mu_0}\right)(\mathbf{m} \cdot \nabla)\mathbf{B} \quad \text{eq. 1}$$

Where \mathbf{F}_m is the magnetic force, μ_0 is the permeability of the medium, and \mathbf{m} is the magnetic moment of the particle within the gradient of magnetic field, \mathbf{B} .^{13, 16, 23} The magnetic moment of the particle is directly proportional to its volume (for uniformly saturated magnetization), so the relative magnitude of the magnetic force per unit mass is constant for different particle sizes (assuming uniform particle density). On the other hand, the primary flow-derived force in the system, the hydrodynamic drag force, is directly proportional to particle radius for a spherical particle:

$$\mathbf{F}_d = 6 \pi \eta r \Delta \mathbf{v} \quad \text{eq. 2}$$

Where \mathbf{F}_d is the hydrodynamic drag force, η is the fluid viscosity, r is the particle radius, and $\Delta \mathbf{v}$ is the velocity difference in fluid and particle motions.^{4, 16, 23} Because volume and mass scale with the cube of the radius for a sphere of uniform density, the relative hydrodynamic drag force per unit particle mass decreases with increasing particle size.

These equations give insight about the key parameters in magnetic particle capture within the CAR-Wash. As applied magnetic field or particle magnetic moment increase, the magnetic force correspondingly increases to more effectively capture particles. These effects are achieved by using a stronger magnet or particles with a higher magnetization. Slower washing buffer flows decrease hydrodynamic drag forces

pushing particles through the channel, resulting in shorter channel lengths traversed during magnetic migration across the channel width.^{4, 16} Additionally, larger particles experience a greater relative magnetic force compared to hydrodynamic drag force due to the relations discussed for eq. 1 and 2. Therefore, hydrodynamic drag forces opposing magnetically-induced motions across washing buffer streamlines have lower relative magnitudes for larger particles. Other forces like hydrodynamic lift (focusing particles toward equilibrium positions within the washing buffer's flow profile) have lower magnitude in this system compared to the magnetic force and the hydrodynamic drag force. While the lift force may oppose the magnetic force in a particle size-, particle position-, and flow velocity-dependent manner, a detailed mathematical treatment of this phenomena in the washing buffer flow bounded by immiscible, co-flowing oil streams is beyond the scope of this work.^{44, 45}

From these relationships, we can infer that magnetic bead capture is most efficient with 1) high magnetic field, 2) large, highly magnetic particles, and 3) relatively slow washing buffer flow velocity toward the waste stream. These demands must be balanced to provide a practically useful device in the context of washing efficiency, throughput, and versatility.

CAR-Wash Performance Characterization. We first evaluated the module with high ($\geq 20\%$) magnetite content $10\ \mu\text{m}$ diameter particles. This provided both ease of visualization and high effectiveness for the applied magnetic field in translating beads across the channel. Figure 2a and Supplementary Video 01 show a representative example of CAR-Wash operation. As reinjected bead-loaded droplets enter the module ($550\ \text{Hz}$, $141 \pm 1\ \text{pL}$ each), electric field applied across the washing buffer and an adjacent saline electrode channel triggered coalescence. The standard design for the platform also included a second electrode feature nearby to enable washing into lower conductivity buffers, but directly charging the washing buffer most efficiently oriented the electric field to coalescence incoming droplets. Electrocoalescence and local turbulence generated and trapped small satellite volumes, particularly at high frequency, but these micron-sized droplet fragments very rarely contained magnetic beads, especially when using $10\ \mu\text{m}$ particles. Satellites usually flowed out through the waste channel with no discernable effect on performance or bead recovery. After droplet coalescence, beads magnetophoretically traversed the

channel width until reaching the washing buffer-oil co-flow interface, and they were effectively re-encapsulated in washing buffer droplets (560 Hz, 189 ± 2 pL each). Monitoring more than 4,000 beads at input and output droplet frequencies of ~ 500 Hz demonstrated greater than 98% successful bead capture into final droplets.

While obtaining specific droplet frequencies required balancing pressure and flow conditions for the washing buffer, oil, droplet, waste, and sample collection lines, the CAR-Wash could also achieve robust operation across a range of conditions. Adjusting these relative flow rates could independently select droplet frequencies and final droplet size, as shown in Supplementary Video 02. This flexibility may prove beneficial when using beads originating from non-identical sample droplets: relatively faster output frequencies produced more empty droplets and reduced the incidence of bead co-encapsulation from different input droplets. Moreover, changing flow conditions also adjusted magnetic particle trajectories. Faster flows displaced particles further down the magnetophoresis channel region during magnetic migration but did not significantly change migration speed in the direction of the magnet, as shown in Figure S1. From this observation, we hypothesize that effective magnetic particle capture using higher operating frequencies with higher flow rates may be obtainable in the future by lengthening the magnetophoresis channel region correspondingly. In summary, several flow and device parameters influenced operation, but magnetic capture and overall performance were generally quite stable under many different flow conditions, and devices were routinely operated for >1 hour.

Next, the washing efficiency was evaluated. Specifically, we wanted to confirm effective exclusion of free material from the original droplets in the final bead-containing droplets. To test this characteristic, we added 1 mM fluorescein to starting droplets, enabling fluorescent monitoring of the content of the original droplets throughout the module as shown in Figure 2b. Uniformly flowing a 10 μ M fluorescein standard through the device at comparable flow rates provided a reference representing fluorescence intensity at 100-fold dilution. Figure 2c shows the results of plotting time-averaged profiles of the fluorescent channel cross section when operating the module and when collecting the fluorescent reference. Promisingly, the channel's fluorescence intensity became statistically indistinguishable from the reference

even before the position where the channel bifurcated to divert a fraction of the flow into droplet resegmentation (50 μm position vs. 120 μm for channel bifurcation). Interestingly, positions closer to the channel bifurcation showed significantly lower fluorescence intensity compared to the reference, indicating effective dilution greater than 100-fold in final droplets. Although flow rate and geometry adjustments altered the exact channel position corresponding to the 100-fold dilution threshold, this result demonstrated that the CAR-Wash platform provided highly efficient removal of free species.

Compared to related continuously flowing magnetic droplet approaches, the CAR-Wash platform demonstrates a number of advantages. Our technique cannot discretely collect dynamically selectable portions of sample droplets, a feature shown by some tunable droplet splitting approaches,^{31, 33-35} but it exceeds the other capabilities of previous droplet splitting platforms in the context of washing for sample purification. Specifically, exchanging >99% of droplet volume (as confirmed by fluorescent characterization) surpassed even the highest reported proportion of droplet splitting (95%)³⁵ and more closely resembled the continuously flowing washes of co-laminar approaches.^{22, 23} Therefore, highly efficient removal of unbound species was achieved without complex sequential splitting and dilution operations.³⁶ While maintaining bead capture efficiency (>98%) comparable to these technologies, throughput (~500 Hz) was significantly greater than most splitting examples (0.5-30 Hz)^{17, 33-37} and surpassed our previous work in this area (200 Hz).³¹ Compared to Lee *et al.*'s synchronized washing design, our system shows similar advantages in volume exchange (~96% reported) and throughput (3 Hz reported).¹⁴ Importantly for applications with heterogeneous droplets (perhaps containing single cells, etc.), Lee *et al.*'s system discretely paired sample and washing buffer droplets to ensure that beads from unique sample droplets did not mix in final droplets, and we can achieve this result by offsetting input and output droplet frequencies.

CAR-Wash Bead Input Versatility. We next re-engineered the device to accommodate alternative magnetic particles. Depending on properties such as surface coating and binding capacity, bead requirements can vary by assay, and previous magnetic droplet assays have employed a range of particle identities.^{14, 17, 31, 33-37} Therefore, we anticipated highest utility for the CAR-Wash if applicable within the

limitations of other commercially available beads, particularly those with low magnetic content per bead. Figure 3a provides the schematic of the modified CAR-Wash module for handling smaller 2.8 μm Dynabeads with 14% reported magnetite content. The chief modification was the extension of the magnetophoresis region by more than five-fold compared to the original device to compensate for the lower proportion magnetite observed in these particles. Increased residence time for Dynabeads through the extended channel (at relatively fixed flow rates) was necessary to fully capture beads which were less rapidly deflected by the magnet as shown in Figure 3b. Next, Figure 3c shows deflected particles re-encapsulated in new droplets at the end of the magnetophoresis region, and the added flow focusing oil channels stabilized this terminal operation. This added feature was necessary to compensate for less stable flow across the longer co-flow capture region, largely originating from variance in reinjected droplets but exaggerated by the extended co-flow distance. Without the added flow focusing structure, resegmentation of droplets sometimes generated irregular droplet sizes or did not occur at all (co-flow only). Monitoring $N > 1000$ Dynabeads at droplet input and output frequencies ≥ 200 Hz yielded higher than 99% bead recovery. Finally, repeating the fluorescent droplet characterization method described earlier for this device indicated reaching the 100-fold dilution threshold at the 60 μm channel position (with channel bifurcation still occurring at 120 μm , Figure 3d-e). Therefore, this CAR-Wash variant retained the advantages in throughput and waste removal efficiency of the original design in comparison to previous magnetic washing examples while still achieving effective particle capture.^{14, 31, 33-36} In summary, this modification slightly increased footprint and operating complexity, but it established comparable performance for smaller, lower magnetic content particles, widening the device's potential application space and extending general usability.

CAR-Wash Enzyme Inhibition Reversal. Beyond profiling the physical performance of the CAR-Wash approach, we also wanted to demonstrate biochemical utility for the device. As an initial application, we chose to monitor washing-mediated inhibition reversal for β -galactosidase activity in cleaving resorufin- β -D-galactopyranoside to free fluorescent resorufin product. Tethering biotinylated enzyme to the surface of 10 μm streptavidin beads added the magnetic handle, and isopropyl β -D-1-

thiogalactopyranoside (IPTG—a well-characterized non-hydrolyzable substrate analog for β -galactosidase) served as a competitive inhibitor in initial droplets. Therefore, the CAR-Wash module provided a means to wash bead-bound β -galactosidase for IPTG removal. Enzyme activity was monitored through production of fluorescent resorufin, and fully recovered enzyme function relative to uninhibited and inhibited controls indicated successful washing.

Figure 4a outlines the schematic for device operation. Droplets loaded with β -galactosidase-conjugated beads and IPTG were first washed through the original 10 μ m magnetic bead CAR-Wash platform with input and output frequencies near 200 Hz and final droplet volumes between 260 and 300 pL. Output droplets flowed through a short loop of connecting tubing to provide \sim 20 s of incubation while delivering them to a secondary device for dynamic imaging within a planar microchannel. To provide an uninhibited control, Figure 4b shows bright fluorescence in collected droplets during operation without inhibitor in the initial droplets or final washing buffer. Serving as an inhibited control, weakly fluorescent droplets in Figure 4c were continuously exposed to IPTG in both initial droplets and in the final washing buffer. Next, Figure 4d shows bright fluorescence in final droplets when washing away IPTG from the initial droplets. To standardize enzyme loading per droplet, quantitative measurements of droplet intensities in Figure 4e only included data for single bead-containing droplets (circled in red in the images) since droplets with multiple beads appear to have more enzyme than can be inhibited by the provided concentration of inhibitor. Crucially, the washed system with initial IPTG did not differ significantly in fluorescence intensity from the uninhibited control, indicating full enzyme activity after washing. On the other hand, the inhibited control showed significantly lower fluorescence than the two other populations, corresponding to competitive inhibition by IPTG. Because washing succeeded in fully recovering β -galactosidase activity after inhibition, this result verified that the CAR-Wash platform could efficiently remove small molecules in a biologically relevant context.

Selective Protein Enrichment via CAR-Wash. Finally, we wanted to highlight the capabilities of the CAR-Wash platform by demonstrating affinity-based protein enrichment and separation. We chose a HeLa cell line expressing a green fluorescent protein-histone H2B (GFP-H2B) fusion in the nucleus to

provide a target protein to fluorescently monitor and because selective enrichment of chromatin-associated targets provides the basis of many important epigenetic bioassays.²⁴ After manual cell lysis and enzymatic chromatin digestion to increase the accessibility of GFP-H2B, we added mCherry to the cell lysate as an off-target fluorescent protein to be removed during washing in addition to other, non-fluorescent lysate components. Anti-GFP antibody-functionalized magnetic particles selectively captured GFP-H2B prior to magnetic washing. Detection of bead-associated fluorescence in green and red channels indicated the abundance of GFP-H2B and mCherry, respectively, at each stage of the enrichment assay.

Figure 5 includes the workflow for the enrichment assay. First, magnetic beads with surface-tethered anti-GFP antibody were rapidly encapsulated in droplets using a simple flow focusing device at ~ 4 kHz (Figure 5a). This approach reduced a common problem in deploying solid phase particles onto microfluidic assays: gravity-driven settling of dense beads results in a rapid decrease in their effective concentration, preventing efficient loading.⁴⁶ By emulsifying the entire bead population in the span of a few minutes, the beads remained in suspension for subsequent processing. Next, the lysate sample was encapsulated in droplets, and loading the bead emulsion on-chip at high packing fraction enabled electrode-mediated direct injection of beads into lysate droplets (Figure 5b). Bead injection was subject to Poisson statistics and not completely uniform, but integrating sophisticated bead loading approaches in future applications could conceivably ensure uniform bead delivery.⁴⁷ Following off-device incubation to allow for target binding, bead-laden droplets were processed via the original 10 μm bead-handling CAR-Wash (Figure 5c) prior to final imaging. This washing portion of the assay demonstrated another key advantage of the platform. Because the only input requirement for CAR-Wash was that droplets fuse with the washing buffer (which constituted the majority of flow through the module), performance was relatively insensitive to input droplet size and spacing uniformity. In particular, coalescence did not require precise coordination or synchronization between droplet and buffer flows.¹⁴ Therefore, this technology interfaced well with detergent-enabled bioassays, such as the inclusion here of detergent-lysed HeLa in droplets. For other washing approaches, detergent-associated instability and partial channel wetting may cause size or spacing

heterogeneities that disrupt the uniformity of droplet synchronization or compromise control of droplet splitting.

Droplets from each portion of the assay were statically imaged in a planar microchannel (Figure 5d). In both green and red channels, low native fluorescence from antibody-functionalized beads resulted in background signal, but inclusion of GFP-H2B and mCherry when adding cell lysate greatly increased fluorescence intensities before washing, especially the fluorescent signal localized to the surface of the beads via specific and non-specific interactions. After washing, antibody-antigen interactions retained GFP-H2B on bead surfaces while mCherry was washed away, returning red channel fluorescence to background levels. In the green fluorescence channel, significantly higher intensities for pre-wash and post-wash beads compared to the original beads indicated successful GFP-H2B enrichment and retention during washing (Figure 5e). Post-wash beads did have slightly but statistically significantly lower fluorescence than pre-wash beads, suggesting some fraction of sample loss from low antibody-antigen affinity, inconsistent GFP-H2B binding capacity among beads, or the presence of other confounds. Other washing-based droplet assays have reported similar instances of sample loss,^{14,36} so it is clear that future CAR-Wash applications beyond this proof of concept implementation will also require careful optimization to maximize sample capture and retention on magnetic particles. Crucially, red fluorescence from mCherry peaked upon lysate loading before washing, but original beads and beads after washing did not differ significantly from each other in fluorescence intensity (Figure 5f). This result verified that washing effectively removed non-specifically interacting mCherry, returning signal to background levels. Therefore, the CAR-Wash module succeeded in selectively enriching and separating GFP-H2B from mCherry and HeLa lysate components.

Conclusions:

Combining simple, robust operation with high throughput and efficiency, the CAR-Wash platform changes the paradigm for in-droplet solid phase-mediated sample processing. We have characterized system performance in terms of bead loss and final droplet dilution for selected magnetic particles and flow conditions, showing excellent bead recovery and buffer exchange. In optimizing module design, we demonstrated that lengthening the magnetophoresis channel provided a practical strategy for adapting the

system to lower magnetite particles. We have also applied the approach in recovering enzyme activity by washing away a small molecule inhibitor and in selectively enriching a target fluorescent protein from cell lysate. The CAR-Wash platform represents an exciting advance in realizing the promise of droplet microfluidics by narrowing the technological gap between pre-existing droplet methodologies and important (bio)chemical techniques leveraging solid supports. Beyond these initial applications, we anticipate a breadth of downstream technologies capable of high throughput, miniaturized analogs for immunoassays, solid phase extraction, and many others.

Acknowledgements:

We gratefully acknowledge financial support from the National Institutes of Health (NIH CA191186). S.R.D. was supported by a National Science Foundation Graduate Research Fellowship. The authors would like to thank Prof. Tamas Ordog and Dr. Jeong-Heon Lee from the Mayo Clinic Epigenomics Development Laboratory for providing the GFP-H2B expressing HeLa cell line. We also thank Prof. Robert Kennedy (University of Michigan) for access to microfabrication facilities and Nicolas Mesyngier (University of Michigan) for helpful discussions.

Conflicts of Interest:

There are no conflicts to declare.

References:

1. T. Thorsen, R. W. Roberts, F. H. Arnold and S. R. Quake, *Physical Review Letters*, 2001, **86**, 4163-4166.
2. L. Shang, Y. Cheng and Y. Zhao, *Chemical Reviews*, 2017, **117**, 7964-8040.
3. S.-Y. Teh, R. Lin, L.-H. Hung and A. P. Lee, *Lab on a Chip*, 2008, **8**, 198-220.
4. E. Al-Hetlani and M. O. Amin, *Microchimica Acta*, 2019, **186**, 55.
5. H. Song, J. D. Tice and R. F. Ismagilov, *Angewandte Chemie International Edition*, 2003, **42**, 768-772.
6. J.-C. Baret, *Lab on a Chip*, 2012, **12**, 422-433.
7. N. Habib, I. Avraham-Davidi, A. Basu, T. Burks, K. Shekhar, M. Hofree, S. R. Choudhury, F. Aguet, E. Gelfand, K. Ardlie, D. A. Weitz, O. Rozenblatt-Rosen, F. Zhang and A. Regev, *Nature Methods*, 2017, **14**, 955-958.
8. Y. Xu, J.-H. Lee, Z. Li, L. Wang, T. Ordog and R. C. Bailey, *Lab on a Chip*, 2018, **18**, 2583-2592.

9. R. Obexer, A. Godina, X. Garrabou, P. R. E. Mittl, D. Baker, A. D. Griffiths and D. Hilvert, *Nature Chemistry*, 2017, **9**, 50-56.
10. S. M. Prakadan, A. K. Shalek and D. A. Weitz, *Nature Reviews Genetics*, 2017, **18**, 345-361.
11. Z. Zhu and C. J. Yang, *Accounts of Chemical Research*, 2017, **50**, 22-31.
12. T. Trantidou, M. Friddin, Y. Elani, N. J. Brooks, R. V. Law, J. M. Seddon and O. Ces, *ACS Nano*, 2017, **11**, 6549-6565.
13. M. Serra, D. Ferraro, I. Pereiro, J. L. Viovy and S. Descroix, *Lab on a Chip*, 2017, **17**, 3979-3999.
14. H. Lee, L. Xu and K. W. Oh, *Biomicrofluidics*, 2014, **8**, 044113.
15. A. Munaz, M. J. A. Shiddiky and N.-T. Nguyen, *Biomicrofluidics*, 2018, **12**, 031501.
16. M. A. M. Gijs, *Microfluidics and Nanofluidics*, 2004, **1**, 22-40.
17. R. Gao, Z. Cheng, A. J. deMello and J. Choo, *Lab on a Chip*, 2016, **16**, 1022-1029.
18. M. A. Booth, S. A. N. Gowers, C. L. Leong, M. L. Rogers, I. C. Samper, A. P. Wickham and M. G. Boutelle, *Analytical Chemistry*, 2018, **90**, 2-18.
19. C. D. M. Campos, S. S. T. Gamage, J. M. Jackson, M. A. Witek, D. S. Park, M. C. Murphy, A. K. Godwin and S. A. Soper, *Lab on a Chip*, 2018, **18**, 3459-3470.
20. V. Sahore, M. Sonker, A. V. Nielsen, R. Knob, S. Kumar and A. T. Woolley, *Analytical and Bioanalytical Chemistry*, 2018, **410**, 933-941.
21. C. A. G. N. Montalbetti and V. Falque, *Tetrahedron*, 2005, **61**, 10827-10852.
22. A. Q. Alorabi, M. D. Tarn, J. Gómez-Pastora, E. Bringas, I. Ortiz, V. N. Paunov and N. Pamme, *Lab on a Chip*, 2017, **17**, 3785-3795.
23. M. D. Tarn, M. J. Lopez-Martinez and N. Pamme, *Analytical and Bioanalytical Chemistry*, 2014, **406**, 139-161.
24. B. Teste, J. Champ, A. Londono-Vallejo, S. Descroix, L. Malaquin, J.-L. Viovy, I. Draskovic and G. Mottet, *Lab on a Chip*, 2017, **17**, 530-537.
25. A. Ali-Cherif, S. Begolo, S. Descroix, J.-L. Viovy and L. Malaquin, *Angewandte Chemie International Edition*, 2012, **51**, 10765-10769.
26. A. Ray, V. B. Varma, P. J. Jayaneel, N. M. Sudharsan, Z. P. Wang and R. V. Ramanujan, *Sensors and Actuators B: Chemical*, 2017, **242**, 760-768.
27. K. Zhang, Q. Liang, X. Ai, P. Hu, Y. Wang and G. Luo, *Lab on a Chip*, 2011, **11**, 1271-1275.
28. V. Sahore, S. R. Doonan and R. C. Bailey, *Analytical Methods*, 2018, **10**, 4264-4274.
29. P. Garstecki, M. J. Fuerstman, H. A. Stone and G. M. Whitesides, *Lab on a Chip*, 2006, **6**, 437-446.
30. A. R. Abate, T. Hung, P. Mary, J. J. Agresti and D. A. Weitz, *Proceedings of the National Academy of Sciences of the United States of America*, 2010, **107**, 19163-19166.
31. S. R. Doonan and R. C. Bailey, *Analytical Chemistry*, 2017, **89**, 4091-4099.
32. A. Shams Khorrami and P. Rezai, *Soft Matter*, 2018, **14**, 9870-9876.
33. E. Brouzes, T. Kruse, R. Kimmerling and H. H. Strey, *Lab on a Chip*, 2015, **15**, 908-919.
34. B. Verbruggen, T. Tóth, M. Cornaglia, R. Puers, M. A. M. Gijs and J. Lammertyn, *Microfluidics and Nanofluidics*, 2015, **18**, 91-102.
35. B. Verbruggen, K. Leirs, R. Puers and J. Lammertyn, *Microfluidics and Nanofluidics*, 2015, **18**, 293-303.
36. X. Pan, S. Zeng, Q. Zhang, B. Lin and J. Qin, *ELECTROPHORESIS*, 2011, **32**, 3399-3405.

37. D. Lombardi and P. S. Dittrich, *Analytical and Bioanalytical Chemistry*, 2011, **399**, 347-352.
38. S. Wang, K.-J. Sung, X. N. Lin and M. A. Burns, *PLOS ONE*, 2017, **12**, e0173479.
39. D. J. Guckenberger, H. M. Pezzi, M. C. Regier, S. M. Berry, K. Fawcett, K. Barrett and D. J. Beebe, *Analytical Chemistry*, 2016, **88**, 9902-9907.
40. J. Park, G. Destgeer, H. Kim, Y. Cho and H. J. Sung, *Lab on a Chip*, 2018, **18**, 2936-2945.
41. B. Seale, C. Lam, D. G. Rackus, M. D. Chamberlain, C. Liu and A. R. Wheeler, *Analytical Chemistry*, 2016, **88**, 10223-10230.
42. Y. Xia and G. M. Whitesides, *Angewandte Chemie International Edition*, 1998, **37**, 550-575.
43. A. Sciambi and A. R. Abate, *Lab on a Chip*, 2014, **14**, 2605-2609.
44. D. Lee, S. M. Nam, J.-a. Kim, D. Di Carlo and W. Lee, *Analytical Chemistry*, 2018, **90**, 2902-2911.
45. B. P. Ho and L. G. Leal, *Journal of Fluid Mechanics*, 1974, **65**, 365-400.
46. A. K. Price, A. B. MacConnell and B. M. Paegel, *Analytical Chemistry*, 2014, **86**, 5039-5044.
47. M. T. Chung, D. Núñez, D. Cai and K. Kurabayashi, *Lab on a Chip*, 2017, **17**, 3664-3671.

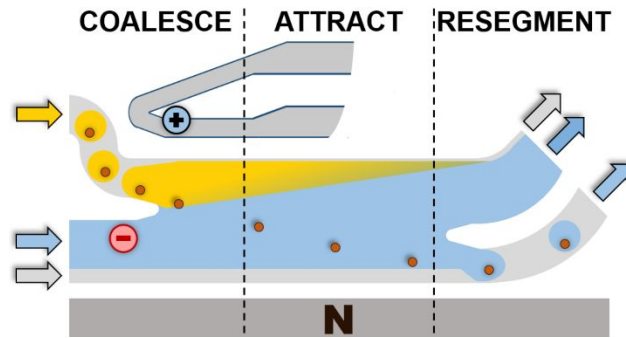


Figure 1. The CAR-Wash technique electrocoalesces input droplets using electric field applied across the washing buffer stream and a nearby ground electrode. Next, a channel-adjacent permanent magnet attracts sample-enriched magnetic beads across the buffer stream while flow forces confine waste material to the original streamline. An oil co-flow prevents bead trapping at the channel wall and, at the end of the module, resegments droplets in washing buffer for further manipulations. Arrows indicate flow directions.

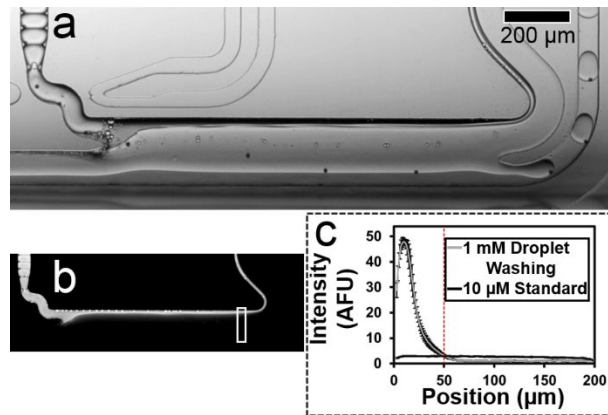


Figure 2. CAR-Wash Operation. a) Micrograph of the module coalescing and resegmenting droplets at >500 Hz each. Electric field was applied across the PBS washing buffer to the adjacent grounded saline electrode channel. The $10\ \mu\text{m}$ magnetic beads are visible as small, black particles, and flow is generally left to right. b) Loading input droplets with fluorescein enables localization of free waste material from input droplets. c) Plot of the intensity of the channel cross-section prior to the bifurcation between the waste stream and the resegmentation stream (region of interest indicated by the white box in the previous image). The fluorescent signal in the channel when washing $1\ \text{mM}$ fluorescein droplets waste material is statistically indistinguishable from a 100-fold diluted standard ($10\ \mu\text{M}$ fluorescein) at position = $50\ \mu\text{m}$ (red dashed line, channel bifurcation occurs at position = $120\ \mu\text{m}$). Error bars on each trace represent 20 fluorescent profiles.

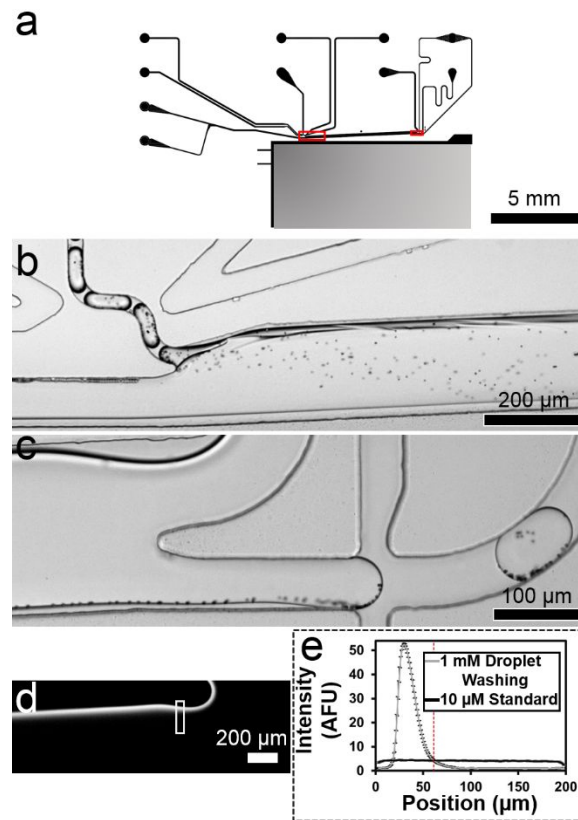


Figure 3. CAR-Wash Application to Alternative Particles. a) Extending the magnetic capture region increases the utility of the module for particles with lower magnetic loading. Red boxes indicate regions of interest shown in following panels. b) Micrograph of the module coalescing input droplets at ~ 250 Hz. Electric field was applied across the PBS washing buffer to the adjacent grounded saline electrode channel. $2.8 \mu\text{m}$ magnetic Dynabeads are evident as small, black particles in high abundance, and flow is generally left to right. c) High magnification micrograph of the module resegmenting droplets downstream at ~ 200 Hz with efficient Dynabead recovery, stabilized by an additional flow focusing structure. d) Loading input droplets with fluorescein enables localization of free waste material from input droplets. e) Plot of the intensity of the channel cross-section prior to the bifurcation between the waste stream and the resegmentation stream (region of interest indicated by the white box in the previous image). The fluorescent signal in the channel when washing 1 mM fluorescein droplets waste material is statistically indistinguishable from a 100-fold diluted standard (10 μM fluorescein) at position = 60 μm (red dashed line, channel bifurcation occurs at position = 120 μm). Error bars on each trace represent 20 fluorescent profiles.

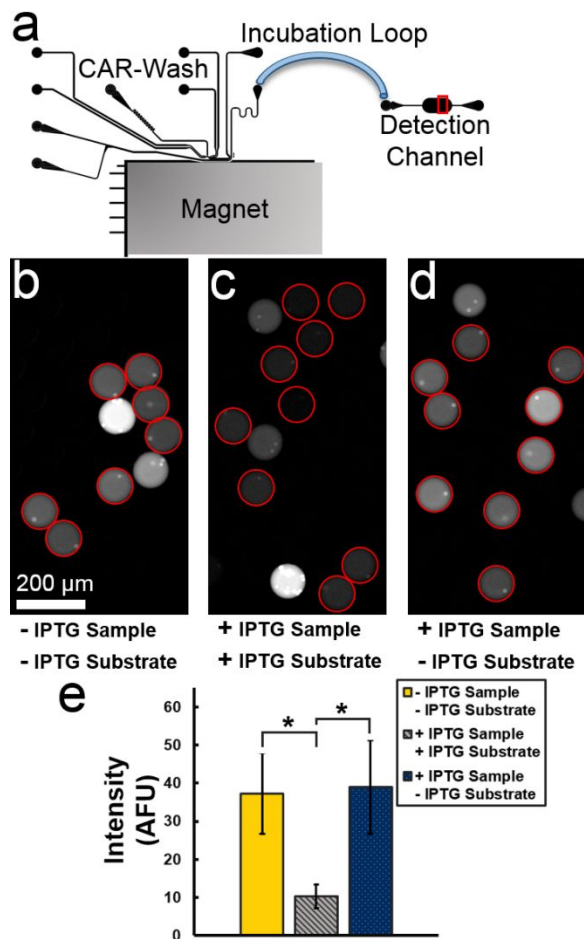


Figure 4. Washing Reverses IPTG Inhibition of β -Galactosidase Activity. a) Droplets containing bead-bound β -galactosidase incubated with 1 mM IPTG were washed into PBS and resorufin- β -D-galactopyranoside substrate using the standard CAR-Wash module. Droplets were imaged on the planar Detection Channel device after ~ 20 s of dynamic incubation accomplished via a 4 cm Incubation Loop of connecting tubing. The red box indicates the region of interest for subsequent images. b) Inhibitor-free control droplets (IPTG neither in original sample droplets nor in final washing buffer with substrate) generated fluorescent resorufin product. Droplets with higher bead loadings typically gave greater signal. c) Inhibited control droplets (IPTG both in original sample droplets and in final washing buffer with substrate) generated little fluorescent product. d) IPTG-containing sample droplets were washed into IPTG-free washing buffer with substrate. Comparable fluorescent product formation relative to the inhibitor-free control indicates inhibitor removal by washing e) Measuring the fluorescence of only single bead droplets (outlined in red) confirmed that washing fully recovered activity in the originally inhibited system (Panel d) compared to uninhibited and inhibited controls (Panels b and c, respectively). The inhibited control (Panel c) differed significantly in intensity from the other conditions.

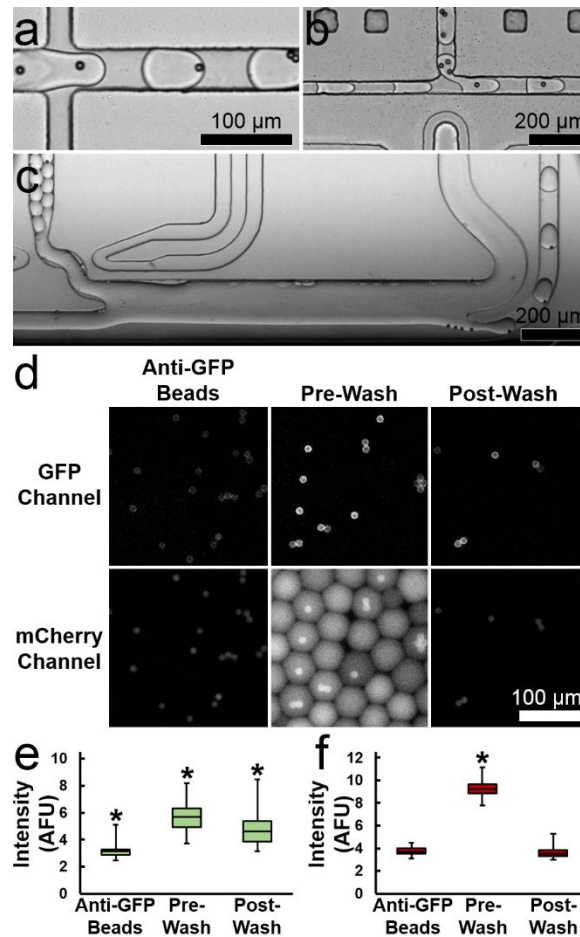
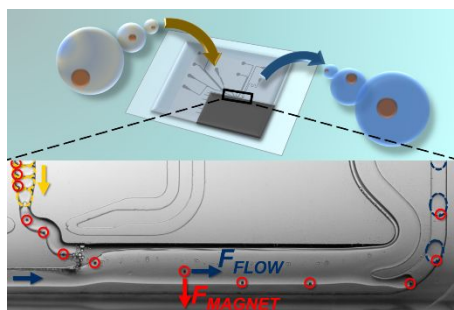


Figure 5. Selective Enrichment of GFP-H2B from Cell Lysate. a) Anti-GFP antibody-functionalized beads were pre-emulsified into droplets at ~ 4 kHz to limit sedimentation. b) The bead emulsion was injected into HeLa cell lysate droplets with added mCherry. c) After 1 hour of off-chip incubation, droplets were processed via the CAR-Wash module. For all devices, flow was generally left to right. d) Droplet populations were fluorescently imaged in green and red channels under static conditions including the functionalized bead emulsion (Anti-GFP Beads), the sample droplets with beads and lysate after incubation but prior to washing (Pre-Wash), and the final sample droplets with beads after washing (Post-Wash). Beads are visible in each panel as bright spots. e) For the green fluorescent channel, the Pre-Wash population was significantly brighter than the original Anti-GFP Beads, indicating the presence of GFP-H2B. Similarly, the Post-Wash population was significantly brighter than the original Anti-GFP Beads, demonstrating enrichment and retention of GFP-H2B after washing. The Post-Wash population was slightly, but significantly less bright than the Pre-Wash population, suggesting incomplete GFP-H2B recovery. f) For the red fluorescent channel, the Pre-Wash population was significantly brighter than the original Anti-GFP Beads due to the presence of mCherry added to the cell lysate. Importantly, the Post-Wash population was not significantly brighter than the original Anti-GFP Beads, indicating mCherry removal by washing.

Table of Contents Figure

The CAR-Wash provides >100 -fold dilution with $>98\%$ magnetic bead recovery for washing picoliter-scale droplets at 500 Hz.